Smart Structures and Systems, *Vol. 34*, *No. 3* (*2024*) *203-213*
https://doi.org/10.12989/sss.2024.34.3.203

Vehicle-induced vibration mitigation of bridges with stiffness degeneration by pounding tuned mass dampers

Xiao-Tong Sun [1a], Zuo-Cai Wang*[1,2], De-An Li [1], Yu Xin [1,3b] and Da-You Duan [1c]

[1] *Department of Civil Engineering*, *Hefei University of Technology*, *Hefei*, *Anhui*, *230009*, *China*
[2] *Anhui Province Infrastructural Safety Inspection and Monitoring Engineering Laboratory*, *Hefei*, *Anhui*, *23009*, *China*
[3] *Anhui Province Engineering Research Center for Civil Engineering Disaster Prevention and Mitigation*, *Hefei*, *Anhui*, *230009*, *China*

(*Received June 7*, *2022*, *Revised October 5*, *2024*, *Accepted October 20*, *2024*)

Abstract. A cracked bridge with reduced stiffness is susceptible to vehicle-induced vibrations above the warning threshold. This study proposes a pounding tuned mass damper (PTMD) with an adjustable mass and double pounding boundaries covered with a viscoelastic material. The PTMD is intended to reduce bridge vibrations caused by vehicle loads. A vehicle-bridge-PTMD coupled equation of motion is established against the engineering background of a continuous steel-concrete composite girder bridge. The bridge performance degradation is evaluated in terms of crack density and stiffness reduction coefficient, which are determined through field crack investigations. The vehicle-induced vibrations of a cracked continuous steel-concrete bridge are then studied while changing the parameters of the designed PTMD. The PTMD effectively reduced the vehicle-induced vibrations of the bridge. The vibration reduction ratio reached 38.9% after applying three PTMDs with a total mass ratio of 2%. On a simply supported steel–concrete composite beam, three PTMDs with a total mass ratio of 2% reduced the vibration amplitudes by 31.4%.

Keywords: pounding tuned mass damper; stiffness degradation; vehicle-bridge vibration; vibration mitigation

1. Introduction

Steel–concrete composite girders have been widely applied in small- to medium-span bridges over the past several decades (Li *et al*. 2023, Rashid and Bahrami 2023, Yu *et al*. 2023). Owing to their open section characteristics, I-shaped steel–concrete composite girders have a more flexible overall stiffness than box-girder bridges. During the operation period, a bridge structure may produce large driving vibrations that affect the driving safety of vehicles and shorten the fatigue life of the bridge (Zhu *et al*. 2014, Jiang *et al*. 2020). In addition, the concrete slab of a steel–concrete composite girder may crack under vehicle loads or environmental corrosion. Crack development further reduces the stiffness of a concrete slab (Guo *et al*. 2019).

Tuned mass dampers (TMDs) are widely used to suppress vibrations of structures (Chen and Kareem 2003, Das and Dey 1992, Warnitchai and Hoang 2006, Li *et al*. 2010, Dai *et al*. 2021, Abdel-Rohman and John 2006, Domaneschi *et al*. 2015, Kontoni and Farghaly 2019). For nearly one century, researchers have formulated TMDs that attenuate various types of excitations, such as human-induced loads, wind loads, and seismic excitations. For instance, Li and Du (2020) proposed a harmonic balance methodology that considers the nonlinearity of TMDs. They showed that their methodology achieves steady-state amplitude of a single degree-of-freedom (DOF) structure. Wang *et al*. (2021a) proposed a semi-active independent variable-mass TMD that mitigates pedestrian-induced bridge vibrations. They developed a wavelet transform-based control algorithm that adapts the mass of the TMD to changes in structural vibration frequencies. Jangid (2022) optimized the damping and frequency of a tuned mass damper-inerter using a numerical searching technique. They demonstrated that their damper-inerter effectively suppresses the dynamic earthquake response of base-isolated structures. They also investigated the influences of the soil condition and isolation frequency on the tuned mass damper-inerter. Niu *et al*. (2018) proposed an eddy-current-damping TMD for large-scale infrastructures. The gap and damping of this novel TMD can be adjusted by installing permanent magnets. In a case study, this vortex-damping TMD reduced the wind vibrations of flexible hangers on a steel arch bridge. Shi and Cai (2018) studied the vibration-reducing effect of a TMD on bridges under two vehicle-load patterns. They concluded that TMDs can reduce both the maximum dynamic displacement and acceleration of the bridge. Miguel *et al*. (2016) obtained the probability distributions of TMD parameters using the maximum entropy principle. They investigated the TMD parameters in vehicle–bridge models with rough roads. To mitigate vehicle-induced vibrations of bridges, researchers have proposed robust design optimizations of TMDs.

Recently, pounding tuned mass damper (PTMD) (Zhang *et al*. 2013, Qu *et al*. 2024), which consists of a tuned mass

*Corresponding author, Ph.D., Professor,
E-mail: wangzuocai@hfut.edu.cn
[a] Ph.D. Student
[b] Ph.D.
[c] Ph.D.

ISSN: 1738-1584 (Print), 1738-1991 (Online)

and two boundaries covered with viscoelastic materials, is designed to mitigate structural vibration. The boundaries limit the vibration of the mass block while the viscoelastic material dissipates the energy of impacts or pounding. In previous studies, the PTMD more effectively dissipated the energy and was more robust than a traditional TMD. For instance, wind-tunnel experiments by Liu *et al*. (2019) verified that PTMDs can effectively reduce single- and multi-mode vortex-induced vibration amplitudes of stay cables. Xiang *et al*. (2024) propose a pendulum-tuned mass damper with geometric nonlinear dampers, presenting a nonlinear model and optimal design strategy that effectively mitigates seismic responses in structures. Wang *et al*. (2021b) designed a tilting PTMD device and examined its vibration control efficiency on single and multi DOF structures during earthquakes. Zhao *et al*. (2018) tested the vibration control efficiency of PTMD on a traffic signal structure and evaluated the parameter sensitivity of vibration suppression of different simple harmonic frequencies by the device. Nevertheless, PTMDs have been rarely applied to the suppression of bridge vibrations caused by vehicles (Yin *et al*. 2018, 2019).

This study proposes a double-boundary PTMD that reduces the vibrations of bridges under vehicle loads. To evaluate the effectiveness of the PTMD in mitigating vehicle-induced bridge vibrations, stiffness reduction is introduced to the analysis. A vehicle–bridge–PTMD coupled equation is established through vehicle–bridge coupling theory and mechanical PTMD principles. A vehicle–bridge–PTMD coupled system model is then established and simulated against the engineering background of a steel–concrete composite girder bridge. Based on the disease investigation results of the bridge, the vibration reduction effect of PTMD was investigated on a bridge with degenerated stiffness. Furthermore, the effect of varying the PTMD parameters on vibration control by the PTMD was analyzed on a steel–concrete composite beam. Numerical simulation and experimental results indicated that the PTMD can appreciably reduce vehicle-induced vibrations of a steel–concrete composite girder bridge.

2. The PTMD model

PTMD is generally applied as a substructure to control the vibration of the main structure (see Fig. 1). By changing the mass and customizing the spring and damper, the PTMD frequency can be adjusted until it closely matches that of the main structure. In addition, the PTMD is equipped with two boundaries that restrict the mass displacement. When the displacement is small, the energy dissipation of the PTMD equals that of a TMD. When the displacement is large, the extra energy is efficiently dissipated through pounding between the mass and boundaries. The energy dissipation of pounding is amplified by viscoelastic materials bonded to the boundaries. Viscoelastic materials share the characteristics of elastic and viscous materials. When pounded, they are elastically deformed and the kinetic energy is transformed into potential energy and then into internal energy through friction work. Both analytical and experimental investigations have demonstrated the higher frequency robustness of PTMDs than of traditional TMDs (Wang *et al*. 2024).

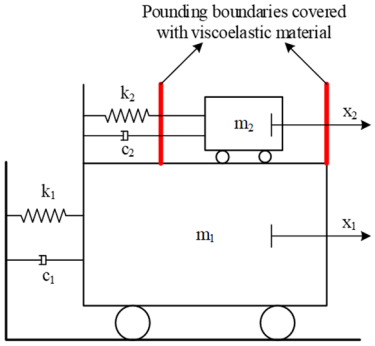

Fig. 1 Schematic of the PTMD model

2.1 The PTMD equation of motion

The PTMD is supposed to be installed at a pivotal position on the bridge, where the response is maximal. The motion equation of the PTMD is

$$\boldsymbol{M_p}\ddot{\boldsymbol{x}}_{\boldsymbol{p}} + \boldsymbol{C_p}\dot{\boldsymbol{x}}_{\boldsymbol{p}} + \boldsymbol{K_p}\boldsymbol{x_p} = \boldsymbol{F_p} + H\boldsymbol{\Gamma P} \tag{1}$$

Where $\boldsymbol{M_p}$, $\boldsymbol{C_p}$, $\boldsymbol{K_p}$ and $\boldsymbol{x_p}$ are the mass, damping, stiffness, and displacement of the PTMD, respectively, and $\boldsymbol{F_p}$ is the external force acting on the PTMD. $\boldsymbol{P}$ is the pounding force, which is nonlinear because it considers the energy dissipated through the collision process. $\boldsymbol{\Gamma}$ and H are the location matrix and direction of $\boldsymbol{P}$, respectively.

2.2 The pounding force model

Impact-force models such as the linear spring model, Kelvin model, and Hertz contact model have been studied in recent years. In the present study, pounding of the PTMD is described by a nonlinear viscoelastic model (Li *et al*. 2015) and the pounding force $\boldsymbol{P}$ is expressed as

$$\boldsymbol{P} = \begin{cases} \beta\zeta(t)^{3/2} + c\dot{\zeta} & \zeta(t) > 0, \dot{\zeta} > 0 \\ \beta\zeta(t)^{3/2} & \zeta(t) > 0, \dot{\zeta} < 0 \\ 0 & \zeta(t) < 0 \end{cases} \tag{2}$$

Where $\zeta(t) = x_1 - x_2 - g_p$ is the relative pounding deformation, x_1 and x_2 are the displacements of the boundary and the mass block, respectively, g_p is the gap between the boundary and the mass block, $\dot{\zeta}$ and β are the relative velocity and stiffness coefficient of pounding, respectively, and c is the impact damping.

The damping impact c varies because the viscoelastic material is nonlinear. It is computed as

$$c = 2\xi\sqrt{\beta\sqrt{x_1 - x_2 - g_p}\frac{m_1 m_2}{m_1 + m_2}} \tag{3}$$

With

$$\xi = \frac{9\sqrt{5}}{2}\frac{1-e^2}{e[e(9\pi-16)+16]} \tag{4}$$

Where ξ is the impact damping ratio, which is correlated with the coefficient of restitution e, and m_1 and m_2 are the masses of the colliding bodies. e defines the relationship between the post-impact and prior-impact relative velocities and depends only on the material properties of the colliding bodies. Its value ranges from 0 (fully plastic impact) to 1 (fully elastic impact) (Yin *et al.* 2018). The coefficient e of the viscoelastic material covering the boundaries can be studied in free pounding experiments. Measuring the relative velocities of the colliding bodies before and after the collision, e can be calculated as follows (Jankowski 2010)

$$e = \frac{v'}{v} \tag{5}$$

where v' and v respectfully denote the post-impact and prior-impact relative velocities. In this study, only one type of viscoelastic material was used in the experiments. Since its material properties remain unchanged, e can be considered a constant.

3. The vehicle-bridge-PTMD coupled system model

3.1 The vehicle equation of motion

To simplify the solution of vehicle-bridge coupled vibration equation, the vehicle and bridge are regarded as two independent systems.

The vehicle model consists of one main body and three axle suspension–wheel masses, as shown in Fig. 2. Springs and dampers simulate the connections between the wheel and axle suspensions and between the axle suspensions and vehicle body. The vehicle has nine degrees of freedom: vertical displacement (z_b), pitching rotation (θ_b), rolling rotation (ϕ) of the main body, and the vertical displacements z_i (i =1, 2, …6) of six wheels. The motion equation of the vehicle is given by

$$\boldsymbol{M_v}\ddot{\boldsymbol{z}}_v + \boldsymbol{C_v}\dot{\boldsymbol{z}}_v + \boldsymbol{K_v}\boldsymbol{z}_v = \boldsymbol{F}_G + \boldsymbol{F}_v \tag{6}$$

Where $\boldsymbol{M_v}$, $\boldsymbol{C_v}$, $\boldsymbol{K_v}$, $\mathbf{z}_v$, and $\boldsymbol{F}_G$ are the mass, damping, stiffness, displacement, and gravity force of the vehicle, respectively, and $\boldsymbol{F}_v$ denotes the wheel–road contact forces.

In this study, the vehicle is a three-axle dump truck modeled in Universal Mechanism software (see Fig. 3). The main body has a mass of m = 19,900 kg and rotations I_{xx} = 19460 kg·m^2 and I_{yy} = 134680 kg·m^2. Suspension systems 1, 2 and 3 weigh 490 kg, 808 kg and 653 kg, respectively. The other truck parameters are presented in Table 1.

3.2 The bridge equation of motion

The equation of motion of the bridge is given by

$$\boldsymbol{M_b}\ddot{\boldsymbol{z}}_b + \boldsymbol{C_b}\dot{\boldsymbol{z}}_b + \boldsymbol{K_b}\boldsymbol{z}_b = \boldsymbol{F_b} \tag{7}$$

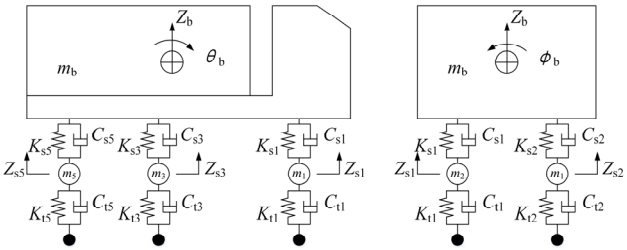

Fig. 2 Schematics of the 9-DOF vehicle model

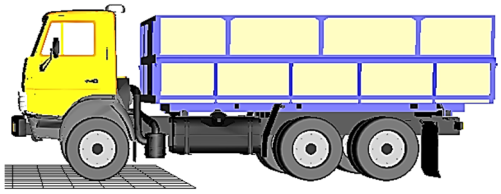

Fig. 3 Truck model developed in Universal Mechanism software

Table 1 Parameters of the truck

	Spring stiffness (N/m)		Damping coefficient (N·s/m)	
	Primary suspension	Secondary suspension	Primary suspension	Secondary suspension
First axle	875082	242604	2000	2190
Second axle	3503307	1903172	2000	7882
Third axle	3507429	1969034	2000	7182

Where $\boldsymbol{M_b}$, $\boldsymbol{C_b}$, $\boldsymbol{K_b}$ and $\boldsymbol{z_b}$ are the mass, damping, stiffness, and displacement of the bridge, respectively, and $\boldsymbol{F_b}$ is the external force acting on the bridge. The bridge structure parameters $\boldsymbol{M_b}$, $\boldsymbol{C_b}$ and $\boldsymbol{K_b}$ can be extracted by establishing a finite element model of the bridge.

3.3 Establishment of the vehicle–bridge–PTMD coupled system

Based on the PTMD, bridge, and vehicle motion equations and the displacement and interaction-force relationships between the bridge and tires, the vehicle-bridge-PTMD coupled system is established as

$$\begin{bmatrix} \boldsymbol{M_b} & \square & \square \\ \square & \boldsymbol{M_p} & \square \\ \square & \square & \boldsymbol{M_v} \end{bmatrix}\begin{Bmatrix} \ddot{\boldsymbol{x}}_b \\ \ddot{\boldsymbol{x}}_p \\ \ddot{\boldsymbol{x}}_v \end{Bmatrix} + \begin{bmatrix} \boldsymbol{C_b} & \boldsymbol{C_{b-p}} & \boldsymbol{C_{b-v}} \\ \boldsymbol{C_{p-b}} & \boldsymbol{C_p} & \boldsymbol{0} \\ \boldsymbol{C_{v-b}} & \boldsymbol{0} & \boldsymbol{C_v} \end{bmatrix}\begin{Bmatrix} \dot{\boldsymbol{x}}_b \\ \dot{\boldsymbol{x}}_p \\ \dot{\boldsymbol{x}}_v \end{Bmatrix} + \begin{bmatrix} \boldsymbol{K_b} & \boldsymbol{K_{b-p}} & \boldsymbol{K_{b-v}} \\ \boldsymbol{K_{p-b}} & \boldsymbol{K_p} & \boldsymbol{0} \\ \boldsymbol{K_{v-b}} & \boldsymbol{0} & \boldsymbol{K_v} \end{bmatrix}\begin{Bmatrix} \boldsymbol{x}_b \\ \boldsymbol{x}_p \\ \boldsymbol{x}_v \end{Bmatrix} = \begin{Bmatrix} \boldsymbol{F_b} \\ \boldsymbol{F_p} + H\boldsymbol{\Gamma P} \\ \boldsymbol{F_v} \end{Bmatrix} \tag{8}$$

where $\boldsymbol{C_{b-v}}$ and $\boldsymbol{K_{b-v}}$ are the damping and stiffness contributing to bridge vibrations from the vehicle, respectively, and $\boldsymbol{C_{v-b}}$, $\boldsymbol{K_{v-b}}$, $\boldsymbol{C_{b-p}}$, $\boldsymbol{K_{b-p}}$, $\boldsymbol{C_{p-b}}$ and $\boldsymbol{K_{p-b}}$ are defined similarly.

Table 2 Classification of road roughness

Classifications class	Ranges of S_q (n_0) (10^{-6}m^3/cycle)	Geometric mean of $S_q(n_0)$
A	2~8	4
B	8~32	16
C	32~128	64
D	128~512	256
E	512~2048	1024

3.4 The road roughness model

The road surface profile can be assumed as an approximate Gaussian stationary stochastic process represented by a power spectral density function (Silva 2004). This profile, which is frequently used in current studies (Ma *et al*. 2019, Green and Cebon 1994), is described as

$$S_q(n) = S_q(n_0)\left(\frac{n}{n_0}\right)^{-2} \quad (n_1 < n < n_2) \tag{9}$$

Where the spatial frequency n (cycle/m) ranges between the lower and upper cut-off frequencies n_1 and n_2, respectively, n_0 (here set to $1/2\pi$) is the discontinuity frequency, and $S_q(n_0)$ is the roughness coefficient (m^3/cycle), which depends on the road surface condition. The road surface profile can be generated through the following inverse Fourier transformation of the power spectral density function

$$r(x) = \sum_{i=1}^{N} \sqrt{2S_q(n_i)\Delta n}\cos(2\pi n_i x + \theta_i) \tag{10}$$

Where n_i is the wave number (cycle/m) and θ_i is the random phase angle, which is uniformly distributed from 0 to 2π.

The road-roughness classes formulated by The National Organization for Standardization (ISO 2016) are listed in Table 2.

4. Numerical simulation and parametric study

This section establishes the vehicle–bridge coupled systems with and without PTMD, which will be numerically simulated for subsequent analyses. To study the effectiveness of PTMD in suppressing bridge vibrations, the dynamic responses are calculated and the influence of mass ratio and number of subsystems on the PTMD system is discussed. The bridge is a continuous steel–concrete composite girder bridge composed of four continuous spans, each of length 35 m. The bridge deck is 13.025 m wide and 0.25 m thick. The top and bottom flanges of each steel girder are separated by 1.75 m. Transverse diaphragms are set at 5-m intervals between the two girders. The material properties of the bridge are listed in Table 3 and a finite element model of the bridge is presented in Fig. 4. The total weight of the bridge is 1,007,560 kg. The first mode frequency of the bridge was calculated as 2.78 Hz.

Table 3 Material properties of the bridge

	Young's modulus (E)	Poisson's ratio (ν)	Density (ρ)
Concrete decks	34.5GPa	0.20	2700kg/m^3
Steel girders	206GPa	0.28	7850kg/m^3

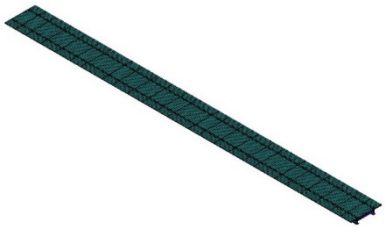

Fig. 4 Finite element model of the bridge

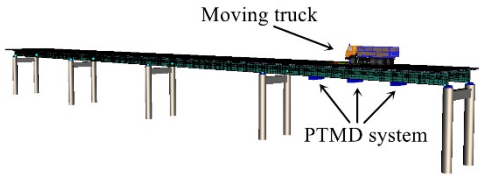

Fig. 5 Model of the vehicle–bridge–PTMD coupled system

The PTMD model was established using the parametric modeling method in Universal Mechanism software. The mass ratio was set to 1% and the PTDM frequency was set to the first mode frequency of the bridge. The damping ratio of the PTMD was obtained by Eqs. (3) and (4). The restitution coefficient *e* and pounding stiffness of the PTMD were set to 0.5 and 20000 N/m$^{3/2}$, respectively.

The dynamic responses of the bridge with a road-roughness of class *C* were studied while the vehicle traveled at 50 km/h. To simulate the driving state of a fully loaded three-axle truck, the vehicle mass was increased to 55 t. The vehicle–bridge coupled system was established by transforming the bridge and vehicle models into subsystems. The dynamic responses at the first mid-span of the bridge were recorded with the PTMD placed at the middle of the first span. The vehicle–bridge–PTMD coupled system is schematized in Fig. 5.

The dynamic responses of the bridge without a PTMD and with one PTMD are plotted in Figs. 6 and 7, respectively. The responses were much stronger without PTMD than when the PTMD system is installed. The maximal responses of the bridge are presented in Table 4. After installing the PTMD, the maximal displacement reduced from 8.056 mm to 6.933 mm. The vibration reduction ratios of the displacement and acceleration were 13.94% and 18.31%, respectively, affirming that the PTMD system effectively mitigates both the displacement and acceleration of the bridge.

4.1 Influence of mass ratio

The mass ratio is a critical determiner of PTMD

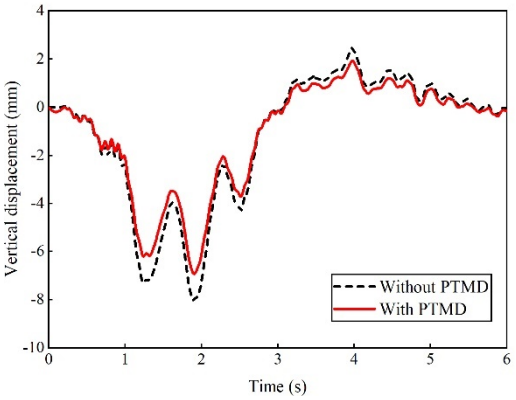

Fig. 6 Displacement responses of the bridge without and with one PTMD

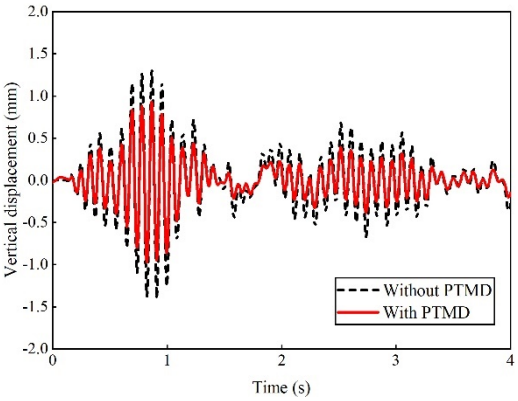

Fig. 7 Acceleration responses of the bridge without and with one PTMD

Table 4 Maximal responses of the bridge without and with a PTMD

	Vertical displacement (mm)	Vibration reduction ratio	Acceleration ($m \cdot s^2$)	Vibration reduction ratio
Without PTMD	8.056	-	1.303	-
With PTMD	6.933	13.94%	1.064	18.31%

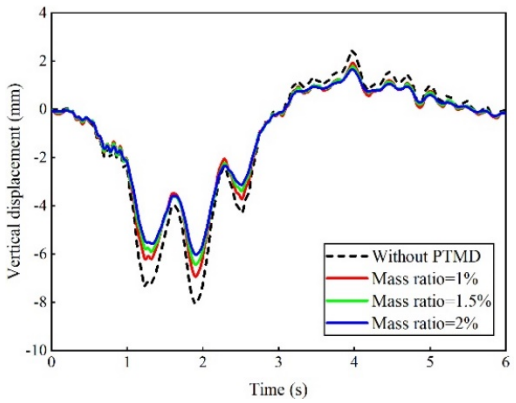

Fig. 8 Displacements of the bridge installed with PTMDs with various mass ratios

Table 5 Vibration reduction performances of PTMDs with various mass ratios

Mass ratio (%)	Maximal displacement (mm)	Vibration reduction ratio
Without PTMD	8.056	——
1.0	6.933	13.94%
1.5	6.435	20.12%
2.0	6.029	25.16%

performance. In general, the efficiency of a PTMD improves with increasing mass ratio. To study the influence of mass ratio on the PTMD, three PTMDs with various mass ratio of 1.0%, 1.5% and 2.0% were designed for the present research. The efficiencies of these three PTMDs were compared in terms of vertical bridge displacement. The displacement time histories are plotted in Fig. 8 and the vibration reduction ratios of each PTMD are listed in Table 5. The mass ratio obviously affects the vibration reduction effect of the PTMD. Increasing the mass ratio from 1% to 2% increased the vibration reduction ratio from 13.94% to 25.16%, indicating a marked improvement in PTMD performance.

4.2 Influence of number of PTMD subsystems

The vibration reduction efficiency of a multiple PTMD (MPTMD) system was discussed in a simulation study. For convenience, each PTMD subsystem was implemented with identical parameters. The total mass ratio of the MPTMD system was set to 2% and the subsystem parameters were designed as described for the single PTMD. The vibration

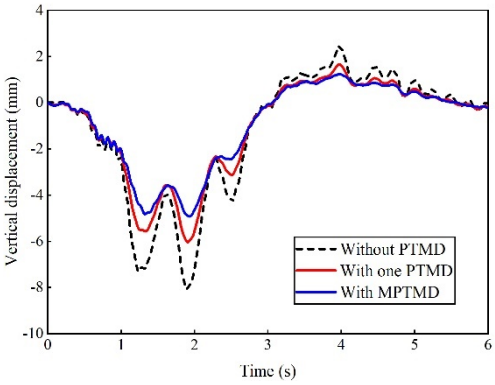

Fig. 9 Displacements of the bridge installed with no PTMD, one TPMD, and multiple PTMDs

Table 6 Comparison of vibration reduction effects of different vibration-suppressed systems

Suppressed system	Maximal displacement (mm)	Vibration reduction ratio
Without suppressed system	8.056	——
PTMD	6.029	25.16%
MPTMD	4.923	38.89%

vibration reduction effect of a MPTMD with three PTMDs was compared with that of a single PTMD. The calculation results are presented in Fig. 9 and Table 6. As evidenced in Table 6, the vibration reduction efficiency of MPTMD exceeded that of a single PTMD. Another noteworthy observation is that multiple low-mass subsystems can avoid the stress concentration caused by a large-mass single PTMD.

5. Vehicle-induced vibration mitigation of a real bridge with stiffness degeneration

This section numerically studies the efficiency of the proposed vibration-mitigation technique on an existing bridge (see Fig. 10). The selected bridge is a continuous steel-concrete composite girder bridge in China consisting of four continuous 35-m-long spans. The bridge deck and I-beam girders are constructed from C40 reinforced concrete and Q345D carbon structural steel, respectively. The bridge parameters are those of the bridge model described in Section 4.

Two disease investigations have been performed on this bridge after service. The investigations revealed gradual cracking of the bridge deck. Figs. 11(a) and (b) are images of typical concrete slabs during the first and second disease investigations, respectively. Obvious cracks appear in the bridge deck and are considerably more numerous in Fig. 11(b) than in Fig. 11(a).

5.1 Stiffness reduction of the bridge

Cracks in the concrete slabs of bridges may occur through environmental corrosion and vehicle loads. Crack development is accompanied by structural degradation of the bridge, which manifests as stiffness degeneration. To quantify the cracking degree of the concrete deck of the bridge, this study introduces a statistical indicator called crack density. First the concrete slab surface was divided into equidistant elements and the number of grids passed by cracks was counted. The crack density was then obtained as the number of cracked grids divided by the total number of grids.

The stiffness of the bridge concrete slab reduces when cracks develop. The stiffness reduction coefficient is related to crack density of the concrete slab as follows

$$\varepsilon = -1.18 \times \eta + 1 \tag{11}$$

Where ε is the stiffness reduction coefficient and η is the statistical crack density. The relationship is plotted in Fig. 12.

The cracking degree of the bridge was evaluated from the results of the disease investigations shown in Fig. 11. The corresponding stiffness reduction coefficients were then calculated by Eq. (11), obtaining ε_1 = 0.7876 and ε_2 = 0.5044 after the first and second disease investigations, respectively. The stiffness reduction coefficients ε_1 and ε_2 were incorporated into two new finite element models of the bridge with the same parameters as the vehicle-bridge coupled system in Section 4. Fig. 13 shows the displacement time histories of the two bridges without the PTMD.

Fig. 10 Photographs of the studied bridge

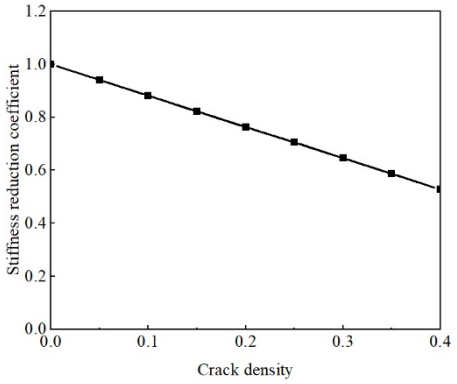

Fig. 12 Relationship between stiffness reduction coefficient and cracking density

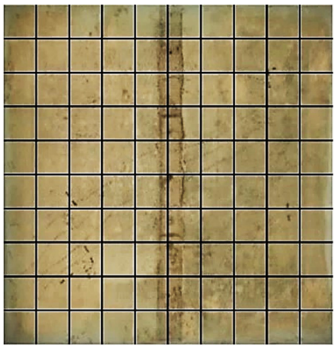

(a) Generally cracked slab

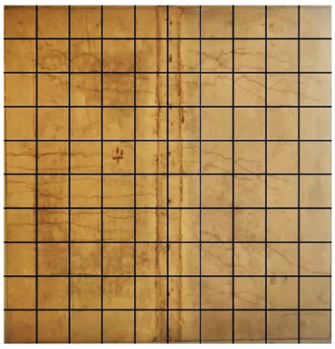

(b) Severely cracked slab

Fig. 11 Cracks in the concrete slabs of a real bridge

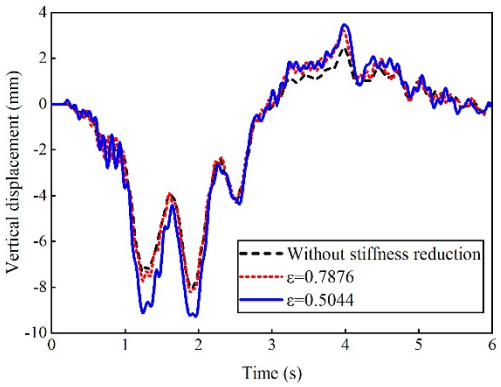

Fig. 13 Displacements of bridges with different degrees of stiffness reduction

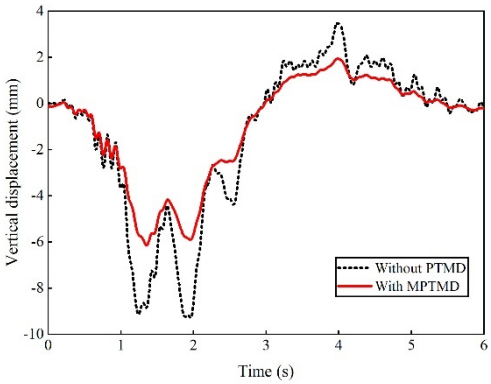

Fig. 15 Displacement of a stiffness-reduced bridge with/ without the PTMD (ε_2 = 0.5044)

Table 7 Maximal displacements of bridges with different stiffness-reduction coefficients

Stiffness reduction coefficient	Maximal displacement (mm)
Without stiffness reduction	8.056
0.7876	8.217
0.5044	9.284

Table 8 Maximal responses of the bridge without and with a vibration suppression system

Degeneration degree	Vertical displacement (mm)		Vibration reduction ratio
	Without PTMD	With PTMD	
ε_1 = 0.7876	8.217	5.068	38.31%
ε_2 = 0.5044	9.284	6.150	33.76%

The maximal displacements are listed in Table 7. Evidently, the bridge vibrations became more serious as the performance became more degraded.

5.2 Effect of PTMD on a bridge with stiffness reduction

To study the vibration reduction effect of MPTMDs on bridges with different degrees of performance degradation, both bridges were installed with a three-PTMD system having a total mass ratio of 2%. The vertical displacements of the bridges with ε_1 = 0.7876 and ε_2 = 0.5044 are presented in Fig. 14, Fig. 15, respectively, and the results of both bridges are summarized in Table 8. When the stiffness reduction coefficients were 0.7876 and 0.5044, the vibration reduction ratios were 38.31% and 33.76%, respectively. This analysis further suggests that MPTMD can suppress vibrations on bridges that are compromised by stiffness reduction.

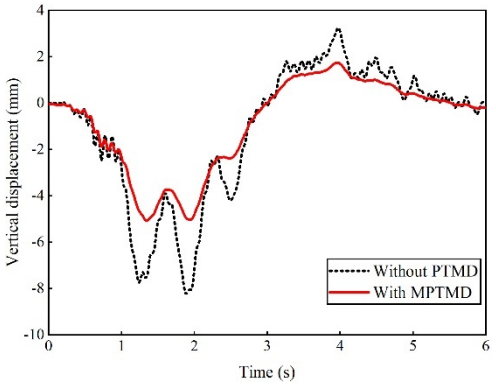

Fig. 14 Displacements of a stiffness-reduced bridge with/ without the PTMD (ε_1 = 0.7876)

6. Experimental verification

6.1 Experimental setup

The efficiency of PTMD was further verified on a simply supported beam. The test beam was 3300 mm long and installed with diaphragms at 400-mm intervals. The deck of the test beam was constructed from C50 concrete and the I-beam was formed from Q345 steel. The test beam weighed 200 kg and its dimensions are given in Fig. 16. The first mode of the test beam was extracted by the block Lansos method in a finite element model of the test beam. The first mode frequency of the test beam was calculated as 12.98 Hz.

The main components of the designed PTMD device were a top plate, two side plates, two limit plates, one connecting plate, four springs, several mass blocks, and viscoelastic materials. To ensure that the quality of the PTMD was controlled mainly by the mass blocks, the plates were formed from aluminum alloy. The mass ratio of the PTMD was adjusted by changing the number of mass blocks. Fig. 17 is a photograph of the PTMD device designed for this experiment. When the test beam vibrated, the mass blocks vibrated under the action of the inertial force and spring, hitting the viscoelastic materials covering the limit plates. The kinetic energy dissipated through the impact was converted to internal energy.

The mass ratio of the PTMD device was selected as 1%. At the optimal damping ratio (6%), the calculated damping value of the PTMD was very small so damping was ignored in the device fabrication. Four springs, each with a stiffness of 695 N/m, were set in each device. Very high bond (VHB) viscoelastic material was used in the designed PTMD.

External excitation was provided by a 100-kg trolley model and the mid-span accelerations and vertical

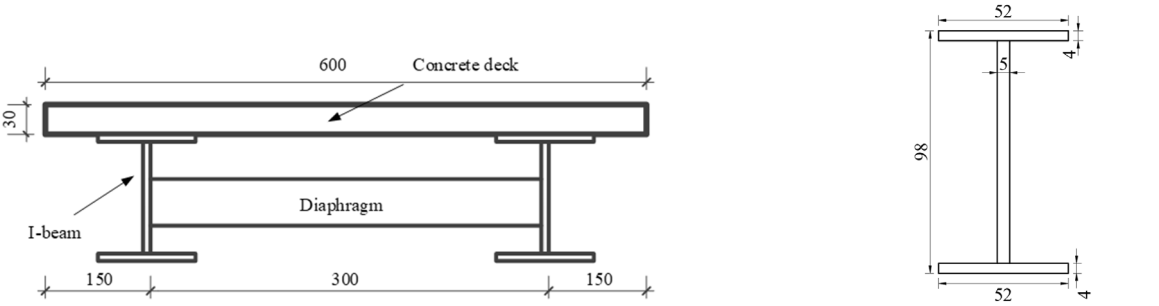

(a) Cross-sections of the test beam (b) Cross-sections of the I-beam

Fig. 16 Dimensions of the designed test beam

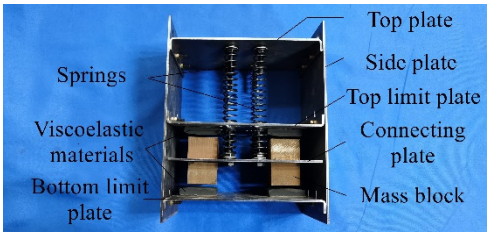

Fig. 17 Photograph of the PTMD device

Fig. 18 Obstacle used in the bump test

Fig. 19 Placement of the whole test system using a simply supported beam

displacements were collected to evaluate the vibration reduction efficiency of the PTMD device. To overcome the speed of the test vehicle effect on the vibration of the tested beam, the trolley was pulled slowly along the test beam during the experimental test. In addition, to amplify the small vibration response of the high-stiffness beam caused by the lightweight trolley, an obstacle was placed on the beam surface as shown in Fig. 18 and a bump test was conducted. In this test, the obstacle size and setting position remained unchanged to ensure constant external loads in multiple groups of tests. Therefore, in this test, the influence of the moving speed of the trolley is weakened, and the vibration response of the test beam is mainly related to the weight of the vehicle and the obstacles on the test beam. During the experiment, the speed of the test vehicle was very slow (nearly zero) when it passed over the top of the obstacles, so as to guarantee good comparability in the results of the comparative experiments. Three displacement sensors and three acceleration sensors were arranged at the 1/4, 1/2 and 3/4 spans of the test beam and connected to a signal acquisition system. The whole test system is shown in Fig. 19.

6.2 Vibration mitigation for the test beam with PTMD

6.2.1 A single PTMD

As shown in Fig. 20, a single PTMD device was installed at the midspan of the test beam with the top plate of the device connected to the beam using anchor bolts. And the trolley was pulled with a traction rope during the bump test. The vibration response of the test beam was monitored in the absence and presence of a PTMD device. Fig. 21 compares the displacement and acceleration responses of the test beam in both cases. The maximal displacement of the test beam at the mid-span was 8.131 mm without the PTMD but reduced to 6.980 mm after installing the PTMD. The vibration reduction ratio was 14.16%, verifying that the PTMD effectively suppressed vibrations of the test beam.

6.2.2 Mass ratio effect

According to the simulation results in subsection 4.1, the mass ratio significantly affects the vibration-reduction performance of a PTMD. To consolidate this finding, the

Fig. 20 The test system using a single PTMD device

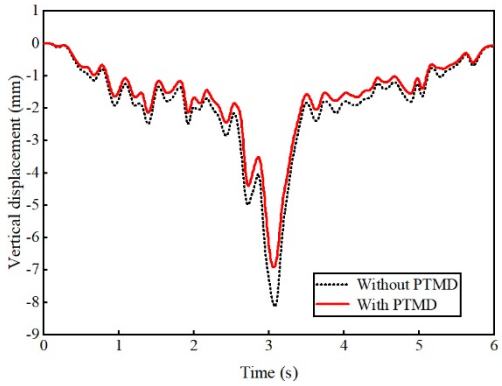

Fig. 21 Mid-span displacement responses of the test beam with and without the PTMD

Table 9 Vibration reduction ratios of PTMDs with different mass ratios

Mass ratio (%)	Maximal displacement (mm)	Vibration reduction ratio (%)
Without PTMD	8.131	—
1	6.980	14.16
2	6.323	22.24

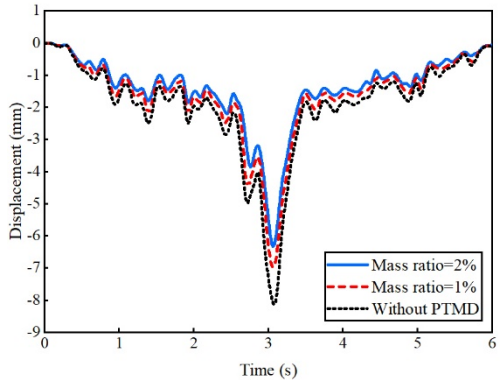

Fig. 22 Displacements of the test beam after installation with PTMDs with different mass ratios

mass ratio of the PTMD device was varied as 1% and 2% and the suppression effect of each PTMD on the vertical displacement was measured at the middle of the test beam. The vibration reduction effects of the two PTMD devices are compared in Table 9.

As clarified in Table 9, the effect of the PTMD device improved with increasing mass ratio. At the maximal displacement, the vibration reduction ratios were 14.16% and 22.24% at mass ratios of 1% and 2%, respectively. The dynamic responses of the test beam installed with each PTMD are compared in Fig. 22.

6.2.3 Number of PTMDs effect

When the total mass ratio is unchanged, MPTMD is more efficient than a single PTMD (see subsection 4.4). This subsection compares the vibration reduction effects of a single PTMD and three PTMD devices with a total mass

Fig. 23 Test beam system using three PTMD devices

Table 10 Design parameters of the PTMD and MPTMD systems

Number of PTMD	Mass ratio (%)	Mass of a single PTMD (kg)	Stiffness of spring (N/m)
1	2	4	5456
3	2	1.33	1902

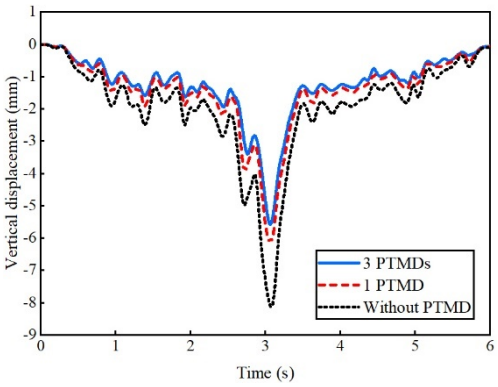

Fig. 24 Displacements of test beam installed with different numbers of PTMDs

Table 11 Efficiencies of the PTMD and MPTMD systems

Number of PTMD	Maximal displacement (mm)	Vibration reduction ratio (%)
Without PTMD	8.131	—
1	6.134	24.56
3	5.579	31.39

ratio of 2%. The aim was to study the impact of varying the number of devices in the beam scenario. As shown in Fig. 23, the PTMD devices were placed at the 1/4, 1/2 and 3/4 span of the test beam.

The parameters of the PTMD devices are shown in Table 10. The vertical displacements and vibration reduction effects of the test beam installed with one and three PTMDs are shown in Fig. 24 and Table 11, respectively. Increasing the number of PTMD devices from one to three obviously reduced the individual PTMD mass and spring stiffness (Table 10). When the total mass ratio was 2%, setting three PTMD devices was more effective

than setting a single PTMD device (Table 11). Therefore, MPTMD can reduce the mass of individual devices and improve the vibration reduction effect. This conclusion has important practical significance for engineering applications of PTMD.

7. Conclusions

In this study, a PTMD device was proposed to reduce the dynamic response of bridges caused by moving vehicles. The vibration reduction effect of the PTMD was investigated in a vehicle–bridge–PTMD coupled system against the engineering background of a steel–concrete composite girder bridge. The effectiveness of the PTMD device was confirmed in experimental and numerical studies. The following conclusions were drawn from the results.

- PTMD can suppress bridge vibrations caused by moving vehicles. Both the mass ratio and number of PTMDs influence the effectiveness of vibration reduction. The designed PTMD also mitigates vibrations of a steel–concrete composite beam.
- The crack density and stiffness reduction coefficient were introduced as quantitative measures of the performance degradation of steel–concrete composite girder bridges. Even when applied to a bridge with reduced stiffness and consequent performance degradation, the PTMD exerts a favorable vibration-reduction effect.
- When the total mass ratio is unchanged, distributing several PTMDs is more effective than applying a single PTMD. In applications, multiple low-mass PTMD subsystems can reduce the adverse impact of adding a large mass to the main structure of the suppressed system.

Acknowledgments

This study was partly supported by the National Natural Science Foundation of China under grand No. 51922036, by The Fundamental Research Funds for the Central Universities under grand No. JZ2020HGPB0117, and by the key research and development project of Anhui province under grand No. 1804a0802204. The results and opinions presented in this paper are those of the authors only and they do not necessarily represent those of the sponsors.

References

Abdel-Rohman, M. and John, M.J. (2006), "Control of wind-induced nonlinear oscillations in suspension bridges using multiple semi-active tuned mass dampers", *J. Vib. Control*, **12**, 1011-1046. https://doi.org/10.1177/1077546306069035

Chen, X.Z. and Kareem, A. (2003), "Efficacy of tuned mass dampers for bridge flutter control", *J. Struct. Eng.*, **129**, 1291-1300. https://doi.org/10.1061/(ASCE)0733-9445(2003)129:10(1291)

Dai, J., Xu, Z.D., Gai, P.P. and Xu, Y.W. (2021), "Mitigation of vortex-induced vibration in bridges using semiactive Tuned Mass Dampers", *J. Bridge Eng.*, **26**, 05021003. https://doi.org/10.1061/(ASCE)BE.1943-5592.0001719

Das, A.K. and Dey, S.S. (1992), "Effects of tuned mass dampers on random response of bridges", *Comput. Struct.*, **43**, 745-750. https://doi.org/10.1016/0045-7949(92)90518-5

Domaneschi, M., Martinelli, L. and Po, E. (2015), "Control of wind buffeting vibrations in a suspension bridge by TMD: hybridization and robustness issues", *Comput. Struct.*, **155**, 3-17. https://doi.org/10.1016/j.compstruc.2015.02.031

Green, M.F. and Cebon, D. (1994), "Dynamic response of highway bridges to heavy vehicle loads: theory and experimental validation", *J. Sound Vib.*, **170**, 51-78. https://doi.org/10.1006/jsvi.1994.1046

Guo, Z.Z., Ma, Y.F., Wang, L. and Zhang, J.R. (2019), "Modelling guidelines for corrosion-fatigue life prediction of concrete bridges: considering corrosion pit as a notch or crack", *Eng. Fail. Anal.*, **105**, 883-895. https://doi.org/10.1016/j.engfailanal.2019.07.046

ISO (2016), Mechanical vibration-road surface profiles-reporting of measured data; International Organization for Standardization, Geneva, Switzerland.

Jangid, R.S. (2022), "Optimum parameters and performance of tuned mass damper-inerter for base-isolated structures", *Smart Struct. Syst., Int. J.*, **29**(4), 549-560. https://doi.org/10.12989/sss.2022.29.4.549

Jankowski, R. (2010), "Experimental study on earthquake-induced pounding between structural elements made of different building materials", *Earthq. Eng. Struct D.*, **39**(3), 343-354. https://doi.org/10.1002/eqe.941

Jiang, C., Wu, C., Cai, C.S. and Xiong, W. (2020), "Fatigue analysis of stay cables on the long-span bridges under combined action of traffic and wind", *Eng. Struct.*, **207**, 110212. https://doi.org/10.1016/j.engstruct.2020.110212

Kontoni, D.P.N. and Farghaly, A.A. (2019), "Mitigation of the seismic response of a cable-stayed bridge with soil-structure-interaction effect using tuned mass dampers", *Struct. Eng. Mech., Int. J.*, **69**(6), 699-712. https://doi.org/10.12989/sem.2019.69.6.699

Li, L. and Du, Y. (2020), "Design of Nonlinear tuned mass damper by using the Harmonic Balance Method", *J. Eng. Mech.*, **146**, 04020056. https://doi.org/10.1061/(ASCE)EM.1943-7889.0001776

Li, Q., Fan, J., Nie, J., Li, Q. and Chen, Y. (2010), "Crowd-induced random vibration of footbridge and vibration control using multiple tuned mass dampers", *J. Sound Vib.*, **329**, 4068-4092. https://doi.org/10.1016/j.jsv.2010.04.013

Li, L., Song, G., Singla, M. and Mo, Y.L. (2015), "Vibration control of a traffic signal pole using a pounding tuned mass damper with viscoelastic materials (II): Experimental verification", *J. Vib. Control*, **21**, 670-675. https://doi.org/10.1177/1077546313488407

Li, D., Nie, J.H., Wang, H., Yan, J.B., Hu, C.X. and Shen, P. (2023), "Damage location, quantification and characterization of steel-concrete composite beams using acoustic emission", *Eng. Struct.*, **283**, 115866. https://doi.org/10.1016/j.engstruct.2023.115866

Liu, M., Yang, W., Chen, W. and Li, H. (2019), "Experimental investigation on multi-mode vortex-induced vibration control of stay cable installed with pounding tuned mass dampers", *Smart Struct. Syst., Int. J.*, **23**(6), 579-587. https://doi.org/10.12989/sss.2019.23.6.570

Ma, L., Zhang, W., Han, W.S. and Liu, J.X. (2019), "Determining the dynamic amplification factor of multi-span continuous box girder bridges in highways using vehicle-bridge interaction analyses", *Eng. Struct.*, **181**, 47-59. https://doi.org/10.1016/j.engstruct.2018.11.059

Miguel, L.F.F., Lopez, R.H., Torii, A.J., Miguel, L.F.F. and Beck, A.T. (2016), "Robust design optimization of TMDs in vehicle-bridge coupled vibration problems", *Eng. Struct.*, **126**, 703-711. https://doi.org/10.1016/j.engstruct.2016.08.033

Niu, H., Chen, Z., Hua, X. and Zhang, W. (2018), "Mitigation of wind-induced vibrations of bridge hangers using tuned mass dampers with eddy current damping", *Smart Struct. Syst., Int. J.*, **22**(6), 727-741. https://doi.org/10.12989/sss.2018.22.6.727

Qu, G., Liang, Q., Li, L., Bai, X. and Ou, J. (2024), "A novel optimal design method for tuned mass dampers with elastic motion-limiting stoppers", *Earthquake Engng Struct Dyn.*, 1-19. https://doi.org/10.1002/eqe.4232

Rashid, S.P. and Bahrami, A. (2023), "Structural performance of infilled steel–concrete composite thin-walled columns combined with FRP and CFRP: A comprehensive review", *Materials*, **16**(4), 1564. https://doi.org/10.3390/ma16041564

Shi, X. and Cai, C.S. (2008), "Suppression of Vehicle-induced bridge vibration using tuned mass damper", *J. Vib. Control*, **14**, 1037-1054. https://doi.org/10.1177/1077546307082189

Silva, J.G.S. (2004), "Dynamical performance of highway bridge decks with irregular pavement surface", *Comput. Struct.*, **82**, 871-881. https://doi.org/10.1016/j.compstruc.2004.02.016

Wang, L., Nagarajaiah, S., Shi, W. and Zhou, Y. (2021a), "Semi-active control of walking-induced vibrations in bridges using adaptive tuned mass damper considering human-structure-interaction", *Eng. Struct.*, **244**, 112743. https://doi.org/10.1016/j.engstruct.2021.112743

Wang, W., Yang, Z., Hua, X., Chen, Z., Wang, X. and Song, G. (2021b), "Evaluation of a pendulum pounding tuned mass damper for seismic control of structures", *Eng. Struct.*, **228**, 111554. https://doi.org/10.1016/j.engstruct.2020.111554

Wang, W., Lu, C., Chen, S., Chen, B. and Hua, X. (2024), "Damping enhancement of nodal modes for stay cables using a single-sided pounding tuned mass damper (SS-PTMD)", *Eng. Struct.*, **305**, 117659. https://doi.org/10.1016/j.engstruct.2024.117659

Warnitchai, P. and Hoang, N. (2006), "Optimal placement and tuning of multiple tuned mass dampers for suppressing multi-mode structural response", *Smart Struct. Syst., Int. J.*, **2**(1), 1-24. https://doi.org/10.12989/sss.2006.2.1.001

Xiang, X., Tan, P., He, H., Yao, H. and Zheng, X. (2024), "Pendulum tuned mass damper (PTMD) with geometric nonlinear dampers for seismic response control", *J. Sound Vib.*, **570**, 118023. https://doi.org/10.1016/j.jsv.2023.118023

Yin, X., Liu, Y., Song, G. and Mo, Y.L. (2018), "Suppression of bridge vibration induced by moving vehicles using pounding tuned mass dampers", *J. Bridge Eng.*, **23**, 04018047. https://doi.org/10.1061/(ASCE)BE.1943-5592.0001256

Yin, X., Song, G. and Liu, Y. (2019), "Vibration suppression of wind/traffic/bridge coupled system using multiple pounding tuned mass dampers (MPTMD)", *Sensors* (*Basel*), **19**, 1133. https://doi.org/10.3390/s19051133, PubMed: 30845685

Yu, J., Liang, S.L., Ren Z.P., Deng, Y.J. and Fang, J. (2023), "Structural behavior of steel-concrete-steel and steel-ultra-high-performance-concrete-steel composite panels subjected to near-field blast load", *J. Constr. Steel. Res.*, **210**, 108108. https://doi.org/10.1016/j.jcsr.2023.108108

Zhang, P., Song, G., Li, H.N. and Lin, Y.X. (2013), "Seismic control of power transmission tower using pounding TMD", *J. Eng. Mech.*, **139**, 1395-1406. https://doi.org/10.1061/(ASCE)EM.1943-7889.0000576

Zhao, N., Lu, C., Chen, M., Luo, N. and Liu, C. (2018), "Parametric study of pounding tuned mass damper based on experiment of vibration control of a traffic signal structure", *J. Aerosp. Eng.*, **31**, 04018108. https://doi.org/10.1061/(ASCE)AS.1943-5525.0000942

Zhu, J.S., Chen, C. and Han, Q.H. (2014), "Vehicle-bridge coupling vibration analysis based fatigue reliability prediction of prestressed concrete highway bridges", *Struct. Eng. Mech., Int. J.*, **49**(2), 203-223. https://doi.org/10.12989/sem.2014.49.2.203